Segmentation of skin cancer images using an extension of Chan and Vese model

Faouzi Adjed, Ibrahima Faye, Fakhr-Eddine Ababsa

Segmentation of Skin Cancer Images Using an Extension of Chan and Vese Model

Faouzi Adjed*†, Ibrahima Faye*† and Fakhreddine Ababsa‡
*Centre for Intelligent Signal and Imaging Research,
†Department of Fundamental and Applied Sciences,
University Tecknologi PETRONAS, Bandar Seri Iskandar, 32610, Malaysia
‡Laboratoire IBISC EA 4526,
Université D'Evry Val d'Essonne, 91020 Evry - France
Email: faouzi.adjed@gmail.com, ibrahima_faye@petronas.com.my, ababsa@iup.univ-evry.fr

***Abstract*—Recently, more attention is given to automatic detection of cancer. However, the multitude kind of cancer (lung, breast, brain, skin etc.) complicates the detection of this disease with common approaches. An adaptive method for each cancer is the only response to achieve this aim. The segmentation of interest region is the first main step to differentiate between the suspicious and non suspicious part in the image. In this specific work, we focus on a segmentation approach based on Total Variation methods. We propose a generalization of Chan and Vese (CV) model theory and implement it to the particular case of skin cancer images.**

***Keywords*—Skin Cancer, Segemntation, Total Variation, Chan and Vese Model.**

I. Introduction

Melanoma is the most dangerous type of skin cancer, it represents approximately 1.6% of the total number of cancer worldwide [1]. About 132.000 new melanoma saved each year in the world, it has the highest increasing rate compared to other cancer types [2]. In France, 11.176 new melanoma is detected, it takes the 6^{th} rank for women and the 9^{th} for men in 2012 [2]. In Malaysia, skin cancer rates among the fairer-skinned Chinese were approximately 3 times higher than Malay and Indians population [3]. The early detection of skin cancer is the key to treat the tumour successfully.

A. CAD system

Skin cancer has been an attractive topic to researchers since 1984 in computerized analysis of pigment skin lesions [4]. The objective of Computer-Aided Diagnosis (CAD) system is to increase the specificity and sensitivity in melanoma recognition. However, the practical parameters for an automated dermoscopic image classification is still unclear. There are two main shortcoming of the general approach to developing a CAD system for melanoma identification [4]:

1) CAD system is expected to reproduce the decision of pathologists with only the input used by dermatologists.
2) Histopathological data are not available for all lesion, only for those considered suspicious by dermatologists.

Before image acquisition and diagnosis, there is image preprocessing to eliminate artefacts, such as hair or ruler marking [4]. A good result of the image preprocessing facilitate the implementation of the segmentation and the classification methods. The main function of hair-removal algorithm comprises two steps: hair detection and hair repair (restoration). It follows the segmentation step to detect lesion's contours and classification to diagnosis if the the lesion is benign (healthy) or malignant (pathological) using features such as statistical and textural features.

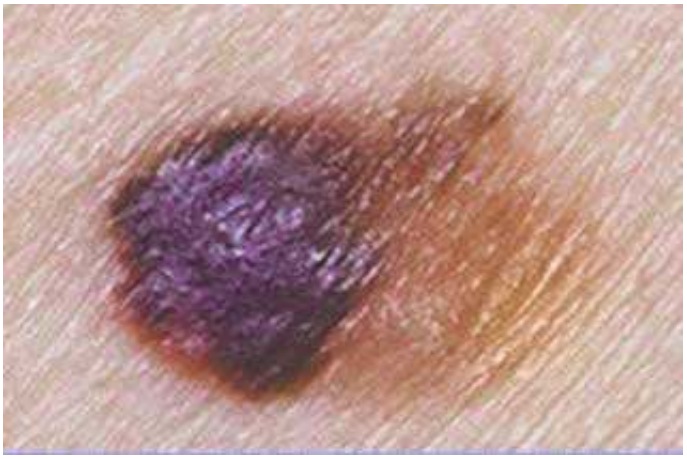

Fig. 1: *Malignant Melanoma [5]*

The life of CAD system consists of the following stages [1]:

1) Image acquisition.
2) Image preprocessing, the main task is the detection and removal of artefacts, especially hairs.
3) Skin lesion segmentation
4) Detection and characterisation of indicators (features).
5) Diagnosis

B. Segmentation

Segmentation is the main stage of detection of skin cancer. The detection of the region of interest with a good performance is hard task for many imaging researchers. Segmentation of melanocytic lesion can be extremely hard. Several methods of

images segmentation were explored. It includes many techniques, such as fuzzy C-means, centre split, multi-resolution, split and merge, PCT/median cut and adaptive threshoding. Many segmentation methods were implemented and tested in skin cancer images [4] .

In [6], the authors used the Color-Based Otsu method, which is simpler and significantly faster for some cases.

Multiresolution representation (e.g. Wavelet, curvelet etc.) have been used in various medical imageprocessing tasks (e.g. [7], [8]). In the particular case of, *Ma et al* in [9] proposed Discrete Wavelet Transform (DWT) to confine signal component to dyadically increasing width frequency bands in different resolutions. Its aim is to discriminate the melanoma's cases. Another method in the area is Ridgelet Transform which was used in [10] for simple images. This approach has a particularity to detect line positions compared to wavelet transform which detects only point positions.

Safi et al in [11] used Total Variation (TV) method developed in [12] which is the generalization of Chan and Vese method [13]. The main idea of this method is to minimize the convex energy of the image. The results of this method are very encouraging. The only problem is that the authors fixed some parameters like λ given in the equation (7) to 2, and in the same time in [12] the value of the same parameter is 0.001.

This paper is demonstrated as follows. The next section presents CV model and some of generalization of this model. In the third section, the proposed method of segmentation wich is kind of generalization of CV model will be presented and developed. In the fourth section, the application of this method in some skin cancer images and the discussion about the obtained results.

II. Chan and Vese model Segmentation

Chan and Vese model is introduced in [13] and its generalization in [14]. The following definition is the one adapted for image segmentation. This method is used to minimize Mumford and Shah equation [15]

Let Ω be open and bounded set and C an evolving curve in Ω. We consider C as a boundary of an open subset ω of Ω, such that $\Omega = \Omega \setminus C \cup \omega \cup C$. The segmentation problem presented in [14] is to solve the following minimization problem:

$$\inf_{u,C}\left\{\int_{\Omega}(u-u_0)^2dxdy+\mu\int_{\Omega\setminus C}|\nabla u|^2dxdy+\nu|C|\right\} \quad (1)$$

where μ, ν are fixed parameters to weight the different terms in the energy (1), $u_0 : \Omega \to \mathbb{R}$ is a given bounded image-function, u is an optimal approximation of u_0 and $|C|$ is the length of curves making C.

A given $C = \partial\omega$ (the boudary of open set $\omega \in \Omega$) is presented implicitly as the zero Lipscitz continuous function $\phi : \Omega \to \mathbb{R}$ such that $\phi(x, y) < 0$ in ω, $\phi(x, y) > 0$ in $\Omega\setminus\omega$ and $\phi(x, y) = 0$ on $\partial\omega$. Using the following Heaviside function $H(z)$.

$$H(z)=\begin{cases}1 & \text{if } z\geq 0\\ 0 & \text{if } z<0\end{cases}$$

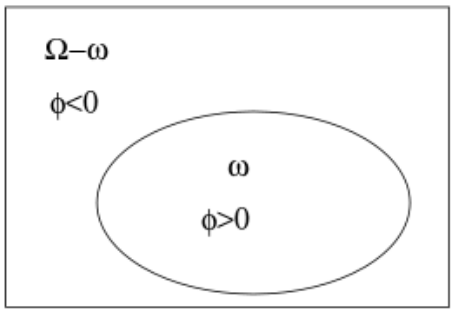

Fig. 2: *The zero level set function. The boundary C is illustrated by the ellipse which is equivalent to $\phi(x, y) = 0$ and it separates the domain Ω into 2 regions $\phi(x, y) > 0$ and $\phi(x, y) < 0$.*

The length of C and the area of ω can be expressed respectively by [14]:

$$|C|=\int_{\Omega}|\nabla H(\phi)|, \quad |\omega|=\int_{\Omega}H(\phi)dxdy \quad (2)$$

Thus, Chan and Vese model is expressed by the following formula [13]:

$$\begin{aligned}F(c_1,c_2) &= \int_{\Omega}(u_0-c_1)^2H(\phi)dxdy\\ &\quad+\int_{\Omega}(u_0-c_2)^2(1-H(\phi))dxdy \quad (3)\\ &\quad+\int_{\Omega}|\nabla H(\phi)|\end{aligned}$$

Where c_1 and c_2 are the averages of u_0 inside the curve C (area of ω) and respectively outside (area of $\Omega \setminus \omega$). These constants (c_1 and c_2) are given by the formula (4) and (5) after approximation and regularization.

Considering H_ε and δ_ε any C^1 approximation and regularization of H and δ_0 function, as $\varepsilon \to 0$ and with $H'_\varepsilon = \delta_\varepsilon$, minimizing the energy, we obtain: $\phi(0, x, y) = \phi_0(x, y)$. The constants c_1 and c_2 are given by the following formula:

$$c_1(\phi) = \frac{\int_{\Omega}u_0(x,y)H_\varepsilon(\phi(t,x,y))dxdy}{\int_{\Omega}H_\varepsilon(\phi(t,x,y))dxdy}, \quad (4)$$

$$c_2(\phi) = \frac{\int_{\Omega}u_0(x,y)H_\varepsilon(1-\phi(t,x,y))dxdy}{\int_{\Omega}H_\varepsilon(1-\phi(t,x,y))dxdy}, \quad (5)$$

In figure (Fig.2), Ω is represented as the square and the ellipse as the curve C, and $\phi(x, y)$ is positive inside and negative outside.

A. Generalization of Chan and Vese model

The first generalization of this method was done by the same authors [14]. Using a union of zero level set functions ϕ_i. The eqaution (3) became:

$$\begin{aligned}F_n(c,\Phi) &= \sum_{1\leq I\leq 2^m}\int_{\Omega}(u_0-c_I)^2\chi_I dxdy\\ &\quad+\sum_{1\leq i\leq m}\nu\int_{\Omega}|\nabla H(\phi_i)|. \quad (6)\end{aligned}$$

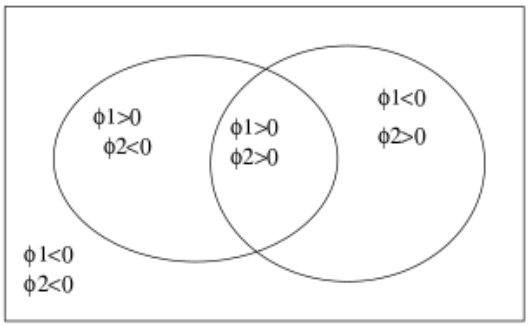

Fig. 3: *C is represented by the 2 curves $\{\phi_1 = 0\} \cup \{\phi_2 = 0\}$ wich gives 4 distinct regions illustrated in this figure, 3 in the foreground and the background.*

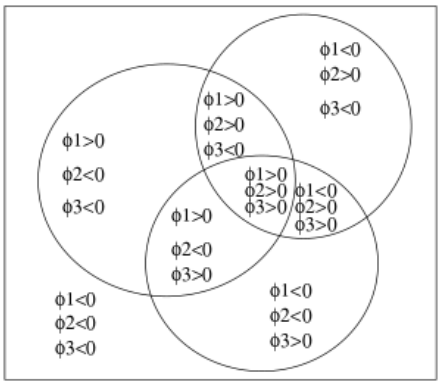

Fig. 4: *C is represented by the 3 curves $\{\phi_1 = 0\} \cup \{\phi_2 = 0\} \cup \{\phi_3 = 0\}$ dived it to 8 regions with the background.*

Where $c = (c_1, c_2, ..., c_n)$ and $\Phi = (\phi_1, \phi_2, ..., \phi_n)$

The figures (Fig. 3) and (Fig. 4) illustrate the cases 2 and 3 zero level sets function respectively. Ellipses and circles represent the curve C respectively and represent the union of $\phi_i = 0$.

Like is noted in [12], this segmentation consider only the cases 2^m, with $m \in \{0, 1, 2, ...\}$. Therefore, for any $m > 2$, at least, one situation N with $N \in]2^{m-1}, 2^m[$ is ignored.

Many researchers are interested by Chan and Vese model and its generalization. Thus, several generalization was studied and developed, in this paper we develop specially the generalization given by *Li et al* [12]. This method was applied specially in skin cancer by *Safi et al* [11], the result are more satisfied compared to other skin cancer result.

In [12], their main work is to find a global formula for each N between 2^{m-1} and 2^m using smooth membership function $u_i \in [0, 1]$. Therefore, the energy given in the equation (1) is reformulated as the following formula:

$$\begin{aligned} F(\{u_i\}_{i=1}^m, \{c_k\}_{k=1}^N) &= \sum_{i=1}^{m} \int_\Omega |\nabla u_i| dx \\ &+ \lambda \sum_{k=1}^{N} \int_\Omega |u_0 - c_k| M_k^N dx \end{aligned} \quad (7)$$

where if $N = 2^m$,

$$M_k^{2^m} = (-1)^{s_k^m} \Pi_{i=1}^m (u_i - b_i^{m,k-1}). \quad (8)$$

otherwise, if $2^{m-1} < N < 2^m$, for $k = 1, ..., 2k_0$:

$$M_k^N = (-1)^{s_k^m} \Pi_{i=1}^m (u_i - b_i^{m,k-1}). \quad (9)$$

and for $k = 2k_0 + 1, ..., N$

$$M_k^N = (-1)^{s_{k_1}^{m_1}} \Pi_{i=1}^m (u_i - b_i^{m_1,k-1}). \quad (10)$$

where $m_1 = m-1$, $k_0 = N-2^{m_1}$, $k_1 = k-k_0$ and $b_i^{m,k-1} = 0 \vee 1$ with $S_k^m = \sum_{i=1}^m b_i^{m,k_1}$.

For $N = 3$, we have the following formula of M_n^k:

$$M_1^3 = u_1 u_2, \quad M_2^3 = u_1(1 - u_2), \quad M_3^3 = 1 - u_1. \quad (11)$$

The equation (11) can be written by zero level set function ϕ used in Chan and Vese model:

$$\begin{aligned} u_1 u_2 &\propto \phi_1 \phi_2 \\ u_1(1 - u_2) &\propto \phi_1(1 - \phi_2) \\ 1 - u_1 &\propto 1 - \phi_1 \end{aligned} \quad (12)$$

We notice that M_1 and M_2 depend both on u_1 and u_2 compared to M_3 which depends only on u_1. The reason given in [11] is to satisfy the constraint of sum of the membership function M_k^N to one given in [16]:

$$\sum_{k=1}^{N} M_k^N = 1$$

In the next section, we explain how and why M_3 can be independent of u_2 using zero level set functions.

III. Proposed Work

The generalization of Chan and Vese model developed in the current work is to find a formulation for each N with $2^{m-1} < N < 2^m$.

The idea of this work is to do the segmentation with not-fixed number of zero level set function ϕ_i. However, for each number of zero set level function ϕ_i, we study all combinations of possible regions which can be detected. In this paper, we study and develop only 2 zero level set functions.

In General case, the energy of minimization given in equation (3) became a minimization of the possible combinations:

$$F_N = \inf_{F_{Ni}} \left\{ \inf_{c,\Phi} F_{Ni} \right\} \quad (13)$$

where $2^{m-1} < N < 2^m$, and i designate the i^{th} combination.

For $m = 2$, we will study the case $N = 3$. The following figures Fig. 5 and Fig. 6 represent the possible cases for $N = 3$, considering the inclusion of ϕ_1 and ϕ_2 is symmetric, i.e $\phi_1 \subset \phi_2$ is equivalent to $\phi_2 \subset \phi_1$.

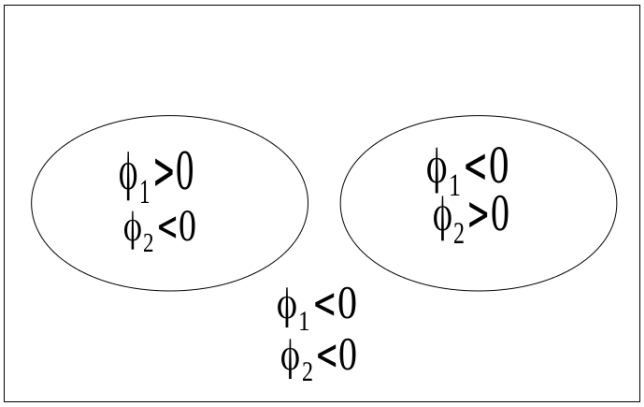

Fig. 5: *C is represented by the 2 curves without intersection between ϕ_1 and ϕ_2. It illustrates one possible case of $N = 3$.*

The energy represented in Fig. 5 and Fig. 6 are given respectively by F_{31} and F_{32}.

$$\begin{aligned} F_{31}(c,\phi) &= \int_\Omega (u_0 - c_{00})^2 H(\phi_1)H(\phi_2)dxdy \\ &+ \int_\Omega (u_0 - c_{01})^2 H(\phi_1)(1 - H(\phi_2))dxdy \\ &+ \int_\Omega (u_0 - c_{10})^2 (1 - H(\phi_1))H(\phi_2)dxdy \\ &+ \nu \int_\Omega |\nabla H(\phi_1)| + \nu \int_\Omega |\nabla H(\phi_2)| \end{aligned} \quad (14)$$

$$\begin{aligned} F_{32}(c,\phi) &= \int_\Omega (u_0 - c_{00})^2 H(\phi_1)H(\phi_2)dxdy \\ &+ \int_\Omega (u_0 - c_{01})^2 H(\phi_1)(1 - H(\phi_2))dxdy \\ &+ \int_\Omega (u_0 - c_{11})^2 (1 - H(\phi_1))(1 - H(\phi_2))dxdy \\ &+ \nu \int_\Omega |\nabla H(\phi_1)| + \nu \int_\Omega |\nabla H(\phi_2)| \end{aligned} \quad (15)$$

where $c = (c_{00}, c_{01}, c_{10}, c_{11})$, with:

$$\begin{aligned} c_{00} &= \frac{\int_\Omega u_0 H(\phi_1)H(\phi_2)dxdy}{\int_\Omega H(\phi_1)H(\phi_2)dxdy} \\ c_{01} &= \frac{\int_\Omega u_0 H(\phi_1)(1 - H(\phi_2))dxdy}{\int_\Omega H(\phi_1)(1 - H(\phi_2))dxdy} \\ c_{10} &= \frac{\int_\Omega u_0 (1 - H(\phi_1))H(\phi_2)dxdy}{\int_\Omega (1 - H(\phi_1))H(\phi_2)dxdy} \\ c_{11} &= \frac{\int_\Omega u_0 (1 - H(\phi_1))(1 - H(\phi_2))dxdy}{\int_\Omega (1 - H(\phi_1))(1 - H(\phi_2))dxdy} \end{aligned}$$

The union of F_{31} and F_{32} gives the case illustrated in figure fig.3, developed in [14] to detect 4 regions.

The objective is to find the best minimization of the energy of the image given by the two cases illustrated by figures (Fig 5, Fig. 6) for $N = 3$.

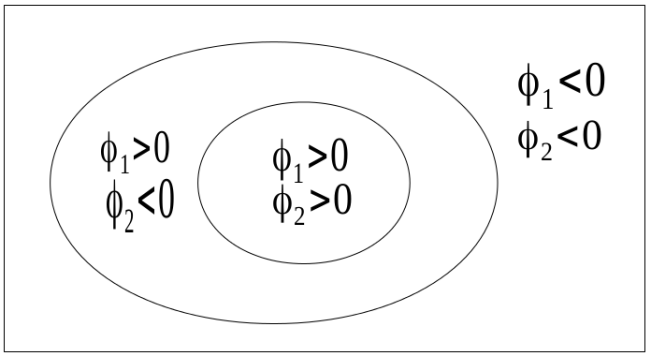

Fig. 6: *C is represented by the overlapping curves. It's illustrated by $\phi_2 \subset \phi_1$ which is symetric to $\phi_1 \subset \phi_2$.*

Thus, the energy to minimize in this case becomes:

$$F_3 = \inf_{F_{31},F_{32}} (\inf_{c,\Phi} F_{31}, \inf_{c,\Phi} F_{32}) \quad (16)$$

Using the equation (14) and (15), the comparison will be only between the third component of each equation, then the equation (16) becomes:

$$\begin{aligned} F_3 &= \int_\Omega (u_0 - c_{00})^2 H(\phi_1)H(\phi_2)dxdy \\ &+ \int_\Omega (u_0 - c_{01})^2 H(\phi_1)(1 - H(\phi_2))dxdy \\ &+ \nu \int_\Omega |\nabla H(\phi_1)| + \nu \int_\Omega |\nabla H(\phi_2)| \\ &+ \inf_{c,\Phi} \Big(\alpha_1, \alpha_2\Big) \end{aligned} \quad (17)$$

where

$$\alpha_1 = \int_\Omega (u_0 - c_{10})^2 (1 - H(\phi_1))(H(\phi_2))dxdy \quad (18)$$

$$\alpha_2 = \int_\Omega (u_0 - c_{11})^2 (1 - H(\phi_1))(1 - H(\phi_2))dxdy \quad (19)$$

The algorithm will not be more complex in computing, because the comparison is only between the different parts (α_1 and α_2). For example, the background of the image will be computed once.

We can simplify the equation given in (19), knowing that $\phi_2 \subset \phi_1$, so if $\phi_1 < 0$ it means automatically $\phi_2 < 0$, then α_2 can be formulated as:

$$\alpha_2 = \int_\Omega (u_0 - c_{10})^2 (1 - H(\phi_1))dxdy$$

This formulation joints M_3 of the equation (11) developed in [12], where it depends only in ϕ_1 (u_1).

IV. Application and Results

In this section, the proposed method and the generalization of CV model given by Vese and Chan [14] in gray and color images are applied and compared. Specially in specific application of skin cancer images.

The development of skin cancer is known by the increasing of the area and variegation of colors in the pigment. The famous method used by medical doctors to detect and recognize

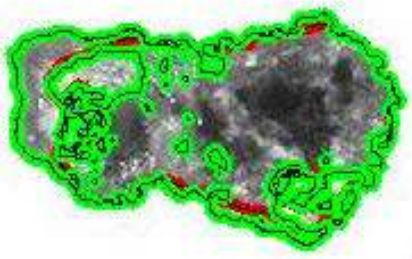

(a)

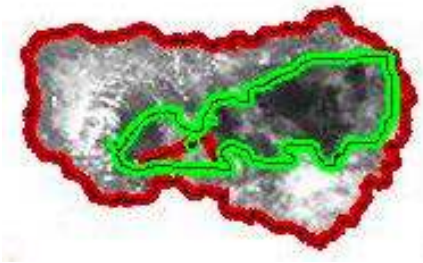

(b)

Fig. 7: *Gray level image. (a): Segmentation by Chan and Vese model. (b): Segmentation by the proposed model .* $\nu = 0.2$

this disease is ABCD rule which is *Asymetry, Border, Color and Diameter* [4], [5]. Until now, almost of CAD explored use ABCD Rule in one block. A separate study of this rule following each component, as color in the current case, is one of the solutions to increase the accuracy of detection.

Usually, skin cancer images are represented by one block with different colors and borders. This dark region mostly is in the middle of the interest region if the development of the pigment is bilateral, and adjacent if the development is only in one side. The following images are implemented by the proposed method and generalized CV model for gray level and color images.

In gray Image, the proposed Method in figure Fig.7-(b) can detect specially the dark region inside the pigment already segmented by the red level set function. But in figure Fig.7-(a), the two level set functions are mixed and the border between the two regions is very confusing. In this case the minimum in the proposed method is F_{32} in the equation (15) illustrated theoretically by the figure Fig.5.

In color case of the same image above (gray level), the result is almost the same. In fact, figures Fig.8-(a) and Fig.8-(b) gives the same result as gray level image segmented in figure Fig.7 by both methods.

In figure Fig.9-(b), the influence of the algorithm is obvious. It's represented by the equation (14), where there isn't any intersection between the two zero level set functions which is illustrated by the figure Fig.6. However, in figure Fig.9-(a) the segmentation by generalized CV model create an additional wrong segmentation coming from the intersection of the two zero level set functions.

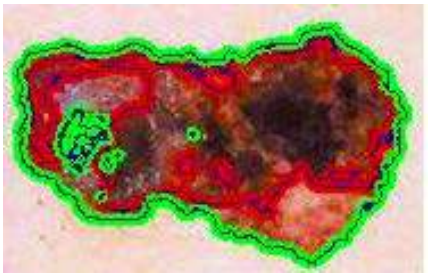

(a)

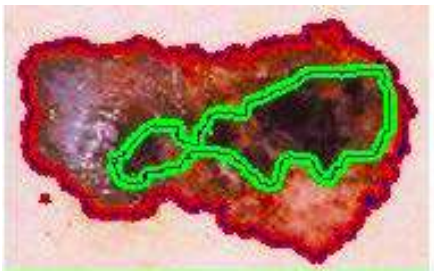

(b)

Fig. 8: *color image. (a): Segmentation by Chan and Vese model. (b): Segmentation by the proposed model.* $\nu = 0.2$

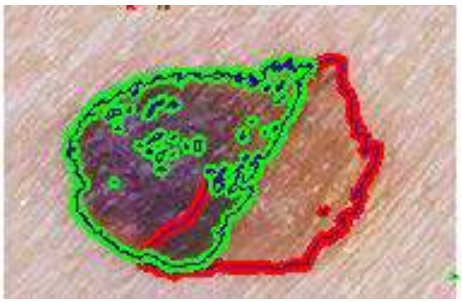

(a)

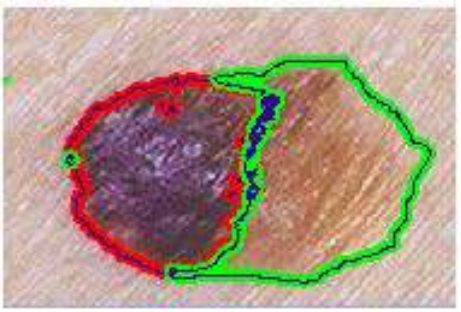

(b)

Fig. 9: *color image. (a): Segmentation by Chan and Vese model. (b): Segmentation by the proposed model.* $\nu = 0.2$

V. Conclusion

In this paper, new approach of the extension of Chan and Vese model and its application in some Skin cancer images is proposed. This extension can be seen like a specification of generalized CV model. With this Approach, the algorithm

forces the two zero level set functions to follow one specific direction, and it becomes less sensible to some small variegation in the pigment. The Algorithm allows the segmentation inside the pigment to detect different colors if development of the disease as inclusion, or separates categorically these functions to make two adjacent regions.

The results shown in the previous section are qualitatively good and more accurate for the detection of the region of interest and the details inside this region.

VI. Acknowledgement

The work is supported by URIF grant 0153AA-B52.

References

[1] J. L. G. Arroyo and B. G. Zapirain, "Detection of pigment network in dermoscopy images using supervised machine learning and structural analysis," *Comput. Biol. Med*, 2013. [Online]. Available: http://dx.doi.org/10.1016/j.compbiomed.2013.11.002

[2] ©Les cancer en France en 2013, *Collection état des lieux et des connaissances, ouvrage collectif édité par l'INCa*, January 2014. [Online]. Available: http://www.e-cancer.fr/Expertises-et-publications/Catalogue-des-publications/Les-cancers-en-France-Edition-2013

[3] M. A. Moore, "Overview of cancer registration research in the asian pacific from 2008-2013," *Asian Pacific Journal of Cancer Prevention*, vol. 14, pp. 4461–4484, 2013.

[4] K. Korotov and R. Garcia, "Computerized analysis of pigmented skin lesion: A review," *Artificial Intelligence in Mdecine*, vol. 56, pp. 69–90, 2012.

[5] M. F. for Medical Education and Research. (2015) Disease and conditions: Skin cancer. [Online]. Available: http://www.mayoclinic.org/diseases-conditions/skin-cancer/multimedia/melanoma/sls-20076095?s=3

[6] G. Capdenhourat, A. Corez, A. Bazzano, R. Allonso, and P. Musé, "Toward a combined tool to assist dermatologists in melanoma detection from dermoscopic images of pigemented skin lesions," *Pattern Recognition Letters*, vol. 32, pp. 2187–2196, 2011.

[7] M. M. M. Eltoukhy, I. Faye, and B. B. Samir, "Using curvelet transform to detect breast cancer in digital mammogram," in *Signal Processing & Its Applications, 2009. CSPA 2009. 5th International Colloquium on*. IEEE, 2009, pp. 340–345.

[8] S. Lahmiri, "A wavelet-wavelet based processing approach for microcalcifications detection in mammograms," *Journal of Advances in Information Technology*, vol. 3, no. 3, pp. 162–167, 2012.

[9] L. Ma and R. C. Stauton, "Analysis of the contour structural irregularity of skin lesion using wavelet decomposition," *Pattern recognition*, vol. 46, pp. 98–106, 2013.

[10] M. N. Do and M. Vetterli, "The finite ridgelet transform for image representation," *IEEE Transaction on Image Processing*, vol. 12, pp. 16–28, 2003.

[11] A. Safi, M. Baust, O. Pauly, V. Castaneda, T. Lasser, D. Mateus, N. Navab, R.Hein, and M. Ziai, "Computer-aided diagnosis of pigmented skin dermoscopic images," *MCBR-CDS*, vol. 7075, pp. 105–115, 2012.

[12] F. Li, C. Shen, and C. Li, "Multiphase soft segmentation with total variation and h^1 regularization," *Math Imaging Vis*, vol. 37, pp. 98–111, 2010.

[13] T. F. Chan and L. A. Vese, "Active contour without edges," *IEEE Transaction on Image Processing*, vol. 10, pp. 266–277, 2001.

[14] L. A. Vese and T. F. Chan, "A multiphaselevel set framework forimage segmentation using the mumford and shah model," *International Journal of Computer Vision*, vol. 50, pp. 271–293, 2002.

[15] D. Mumford and J. Shah, "Optimal approximations by piecewise smooth functions and associated variational problems," *Communications on pure and applied mathematics*, vol. 42, no. 5, pp. 577–685, 1989.

[16] J. Shen, "A stochastic-variational model soft mumford-shah segmentation," *International Journal of Biomedical Imaging*, vol. 2006, pp. 1–14, 2006.